*Engineering Reports*

WILEY

Engineering Reports Open Access

RESEARCH ARTICLE OPEN ACCESS

# Barkhausen Noise- and Eddy Current-Based Measurements for Online Detection of Deformation-Induced Martensite During Flow Forming of Metastable Austenitic Steel AISI 304L

Julian Rozo Vasquez[1] | Hanigah Kanagarajah[1] | Bahman Arian[2] | Lukas Kersting[3] | Werner Homberg[2] | Ansgar Trächtler[3] | Frank Walther[1]

[1]Chair of Materials Test Engineering (WPT), TU Dortmund University, Dortmund, Germany | [2]Forming and Machining Technology (LUF), Paderborn University, Paderborn, Germany | [3]Fraunhofer Institute for Mechatronic Systems Design (IEM), Paderborn, Germany

**Correspondence:** Julian Rozo Vasquez (julian.rozo@tu-dortmund.de)

**Received:** 15 August 2024 | **Revised:** 4 November 2024 | **Accepted:** 18 November 2024

**Funding:** This work was supported by German Research Foundation (Deutsche Forschungsgemeinschaft, DFG) for their support of the depicted research within the priority program SPP 2183 "Property-Controlled Forming Processes," through project no. 424335026 "Property Control During Spinning of Metastable Austenites." The authors thank too the Germany's Federal Ministry for Economic Affairs and Climate Action (BMWK) for funding the project "Development of a corrosion fatigue test rig to investigate the influences of copper-based alloys for hard metal/steel joints and the development of an adapted non-destructive testing methodology" (project no. KK5072219SH1) within the Central Innovation Program for small and medium-sized enterprises (ZIM) managed by AiF Projekt GmbH.

**Keywords:** Barkhausen noise analysis | eddy current | flow forming | micromagnetic testing | non-destructive testing | phase transformation

## ABSTRACT

This paper deals with micromagnetic measurements for online detection of strain-induced α′-martensite during plastic deformation of metastable austenitic steel AISI 304L. The operating principles of the sensors are magnetic Barkhausen noise (MBN) and eddy currents (EC), which are suitable for detection of microstructure evolution due to formation of ferromagnetic phases. The focus of this study was put on the qualification of different micromagnetic techniques and different measurement systems under conditions similar to the real ones during production, which is crucial for implementation of a property-controlled flow forming process. The investigation was carried out on tubular specimens produced by flow forming, which have different content of α′-martensite. To characterize the sensitivity of the sensors, different contact conditions between sensors and workpieces were reproduced. MBN sensors are suitable for detecting amount of α′-martensite, but the measurements are affected by the surface roughness. This entails that the calibration models for MBN sensors must take account of these effects. EC sensors show a closer match with the amount of α′-martensite without having major affectation by other effects.

## 1 | Introduction

The production of components by flow forming has remarkable importance in a wide range of industrial fields such as transportation and aerospace. Flow forming is a promising process, due to manufacturing flexibility, resource optimization, and the possibility to produce high-quality components [1]. The use of metastable austenitic steels as raw material enables the production of components that fulfill geometrical and dimensional requirements with specific properties. During flow forming of

these steels, plastic deformation not only changes the geometry, but also the microstructure of the workpieces. In particular, deformation-induced phase transformation from metastable austenite to α′-martensite may occur, which modifies the magnetic and mechanical properties of the final products [2, 3]. This distinctive attribute of metastable austenitic steels enables the production of tubular parts with a localized gradation of mechanical and magnetic properties. This feature can be exploited to produce parts with enhanced strength and hardness in specific volumes of the workpiece, as well as to imprint invisible magnetic barcode signatures, thereby deterring the falsification of the produced parts. The implementation of online closed-loop control within the production process enables an application-oriented and efficient production of these components [4]. This requires the development of optimal systems for online detection, transmission, and processing of measurements of α′-martensite content. The application of measurement systems operating under magnetic Barkhausen noise (MBN) and eddy current (EC) principles is promising due to their high sensitivity to changes in magnetic properties during the forming process [5, 6], which constitutes a milestone for the property-controlled production of components.

Micromagnetic inspection methods such as MBN and EC can be used as nondestructive testing techniques to characterize the evolution of various properties such as hardness [7–9] and residual stresses [10–12], as well as microstructural features such grain size [13–15], phase transformation [16, 17], and surface damage [18–20]. These techniques have been used to characterize the expected fatigue life [21, 22] and for structural health monitoring investigations [23] by means of the monitoring of the stress state. The literature referenced above is focused on the characterization under laboratory conditions; however, some of these techniques haven been applied directly in production processes. In steel industry, micromagnetic testing has been used for inspection of steel strips [24], quick detection of residual stresses during deep drawing [25], residual stress measurements of inner rings of wheel bearings, and control measurements of graphite composition of car engine crankcases [26]. Various suppliers of micromagnetic inspection systems currently offer online measurement solutions for detecting cracks and manufacturing defects such as grinding burns in axles, camshafts, and gears [27, 28].

The main contribution of this investigation is the qualitative and quantitative evaluation of different measuring systems that operate under MBN and EC principles for detection of amount of α′-martensite in a real flow forming process. The evolution of the magnetic properties due to the transformation of metastable austenite into α′-martensite is closely related with the micromagnetic measurements. Nevertheless, the detailed description of the calibration models is beyond the scope of this paper and has been already published by the authors [29, 30]. The characterization of strain-induced α′-martensite formation by means of micromagnetic techniques has been widely reported in literature [31–33]. However, there are no reported studies about the application of these technologies under real production conditions for a flow forming process. The innovation of this study consists in the generation and analysis of data recorded with different measurement systems to be used in a property-controlled flow forming process. These results are necessary to determine appropriate parameters of the measuring systems, operating windows of the sensors, as well as key features to consider in the further development of calibration models for the sensors and the closed-loop control of the process.

## 2 | Materials and Methods

### 2.1 | Production of Specimens by Means of Flow Forming

The specimens were produced by means of reverse flow forming (Figure 1a) at Forming and Machining Technology of Paderborn University (LUF), using the machine BD 40 (Bohner & Koehle GmbH & Co. KG, Esslingen, Germany). The raw material of the workpieces is seamless tubes made of stainless steel AISI 304L (X2CrNi18-9, 1.4307) with an 80 mm outer diameter and a 4 mm wall thickness. The specimens were manufactured at room temperature, which was kept constant during the production by means of active flooded cooling. The speed rotation of the spindle was 30 rpm and the feed rate of the forming tool was set at 30 mm/min. The flow forming operations were performed using three rollers to reduce the wall thickness of the tubes. The initial 4 mm wall thickness was reduced with infeed depths of 0.75 mm/pass to achieve thickness reductions of 1.50,

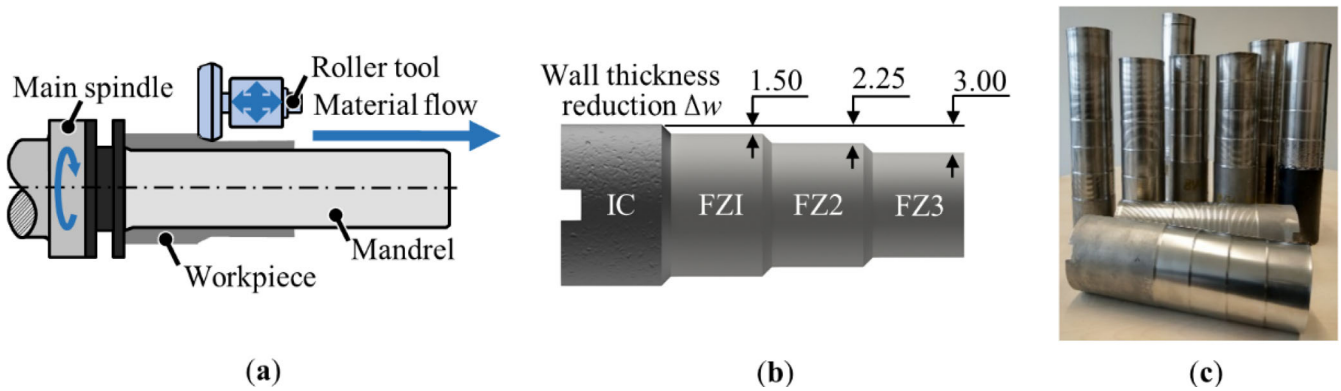


**FIGURE 1** | Specimen manufacture: (a) flow forming process; (b) geometry and dimensions (in mm); (c) final workpieces. FZ: Forming zones 1–3; IC: Initial condition.

2.25, and 3.00 mm. Starting from the initial condition (IC), which is metastable austenite, flow forming operations were performed to produce three forming zones (FZ 1, 2, and 3) (Figure 1b). Each forming zone corresponds to a plastic deformation state with a defined amount of strain-induced α′-martensite. The final specimens manufactured during the production process are shown in Figure 1c.

## 2.2 | Characterization Methods

### 2.2.1 | α′-Martensite, Wall Thickness Reduction, and Roughness Measurements

On the workpiece used for the evaluation of the online detection of α′-martensite amount by means of MBN and EC sensors, offline wall thickness and α′-martensite measurements were carried out. The wall thickness reduction was calculated using thickness measurements performed with the mechanical gauge D4R50 (Kroeplin GmbH, Schluechtern, Germany). The measurements of α′-martensite were recorded by means of the Feritscope FMP30 (Helmut Fischer GmbH, Sindelfingen, Germany). This device works under the magneto-inductive principle to measure the ferritic phase content, which is correlated with the strain-induced α′-martensite, according to [34]. These measurements cannot be used for closed-loop property control, because the online acquisition and real-time transmission of the data to a control system is not possible. As a result, micromagnetic measuring systems are a convenient alternative for indirect detection of α′-martensite amount in property-controlled applications.

Roughness measurements of the different forming conditions of the specimen were carried out by means of the tactile device MarSurf M300 (Mahr GmbH, Goettingen, Germany). The values of arithmetic mean roughness (Ra) of the specimen outer surface were recorded. These measurements are important due to the effect that this workpiece feature has on the micromagnetic measurements [35].

### 2.2.2 | MBN-based Measuring Systems

The setup of a MBN sensor has a magnetization unit formed by a core yoke and a coil, and an additional detection coil. The used frequency controls the penetration depth during testing (Figure 2a). Micromagnetic analyses are based on the behavior of ferromagnetic materials, such as metastable austenitic steel AISI 304L. Ferromagnetic materials are divided in spontaneously magnetized regions called magnetic domains, by means of Bloch walls. During micromagnetic testing a cyclic magnetization and demagnetization of the specimen takes place. In this process, the walls move in response to the applied field. This motion is discontinuous due to the interaction of domain walls with lattice defects, dislocations, phase changes, grain boundaries, and residual stresses. This triggers the Barkhausen effect that can be evidenced in the magnetization hysteresis at high scale (Figure 2b). From the analysis of the hysteresis loop, the MBN profile can be obtained (red profile on Figure 2c). From this curve, parameters such as maximum MBN amplitude ($M_{max}$), mean MBN amplitude ($M_{mean}$), and coercive magnetic field ($H_c$) can be deduced [36–38].

Two measurement systems based in MBN analysis were used to detect the strain-induced α′-martensite by means of specific recorded parameters in the specimens: the 3MA-II (Fraunhofer IZFP, Saarbruecken, Germany) (Figure 3a) and the Rollscan 350 (Stresstech, Vaajakoski, Finland) (Figure 3b). The online MBN analysis with 3MA-II was carried out with a magnetization frequency of 80 Hz, a magnetic field strength of 80 A/cm, and a bandpass filter of 500 kHz to 1 MHz. The recorded parameter used for the analysis is $M_{max}$, which is a parameter tightly correlated with the amount of α′-martensite [29, 35]. On the other

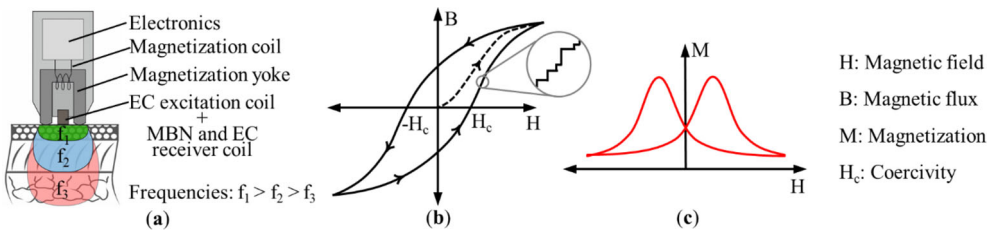


**FIGURE 2** | Magnetic Barkhausen noise analysis: (a) principle setup of MBN probes; (b) hysteresis loop of magnetization of ferromagnetic materials and (c) MBN profile extracted of the magnetization hysteresis.

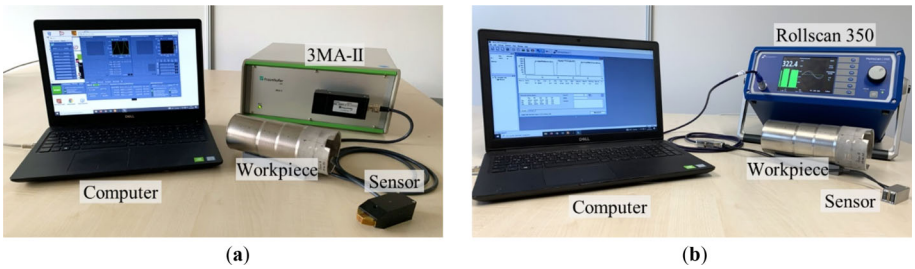


**FIGURE 3** | Magnetic Barkhausen noise-based measuring systems for online detection of the amount of α′-martensite: (a) 3MA-II and (b) Rollscan 350 measuring systems.

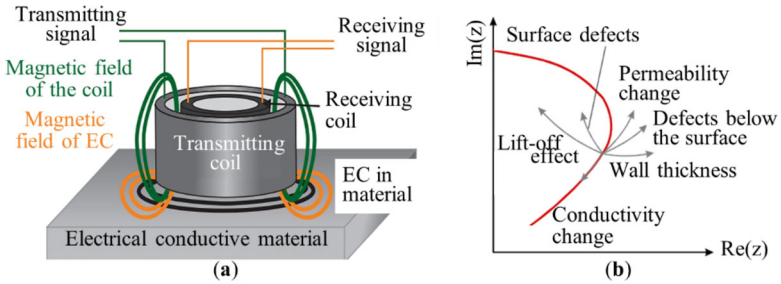


**FIGURE 4** | Eddy current analysis: (a) principle of the EC test method [39] and (b) impedance diagram and correlation with different material features and properties [40].

side, Rollscan 350 delivers the magnetoelastic parameter (mp), which is calculated from individual MBN pulses. The measurements were recorded with a bandpass filter of 70–200 kHz. The magnetization frequency and voltage were chosen by means of an automatic sweep routine of the measuring device. The obtained parameters were 80 Hz frequency and 1.5 $V_{pp}$ voltage. A magnetization frequency of 80 Hz is within the typical range in MBN testing (50–150 Hz) and enables a penetration depth between 2 and 3 mm approximately.

### 2.2.3 | EC-based Measuring Systems

In EC testing, an AC voltage is applied to a transmitter coil to induce a primary alternating magnetic field. This field generates EC in electrically conductive materials, which causes a secondary alternating magnetic field. Factors such as permeability, residual stresses, hardness and defects of the workpiece have an impact on the strength of the EC and of the secondary magnetic field. The interference between the primary and secondary magnetic fields results in a total magnetic field, which induces an alternating voltage in the measuring coil (Figure 4a).

The induced voltage of the measuring coil is called EC signal and is displayed in the complex plane. The plot of the imaginary and real parts of the test coil impedance are correlated with the evolution of properties like conductivity and permeability, as well as features like defects and layer thicknesses (Figure 4b). Since austenite and martensite have different conductivity and permeability, EC measurements are suitable to characterize the amount of α′-martensite [41, 42]. The EC measurements are determined by the test frequency, which controls the penetration depth [40].

The online EC measurements were carried out using two different measurement systems: 3MA-II (Figure 3a), which allows to obtain MBN and EC at the same time, and Elotest PL600 (Rohmann GmbH, Frankenthal, Germany) (Figure 5). The EC signals were recorded in both systems with a frequency of 1 MHz, which is a typical test frequency used in EC testing. With this frequency, an approximate penetration depth between 10 and 15 µm can be reached for tests in austenitic stainless steels after plastic deformation. The measurements of the imaginary and real part of the impedance are used to calculate the phase and amplitude of the measured signals. Since EC testing is a comparative method, an evaluation of the results requires a reference signal, which in this case corresponds to the austenite or IC. To detect the amount of strain-induced α′-martensite in the different forming zones

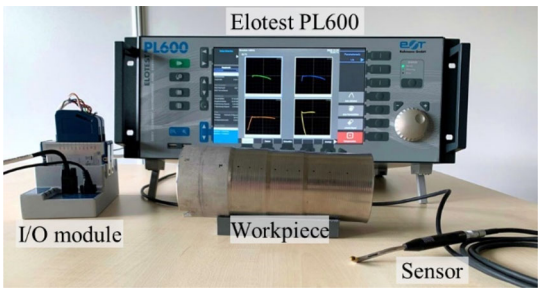


**FIGURE 5** | EC-based measuring system for online detection of the amount of α′-martensite: Elotest PL600 measuring system.

(FZ1 to 3) of the specimen, the distance between the EC signals of IC and the different FZ was calculated by means of statistical variance. This distance is called the modulus $\Delta m$, which is reported in the results. For the sake of comparison, the higher $\Delta m$, the greater the amount of strain-induced α′-martensite.

## 2.3 | Determination of the Measuring Spot Size of the MBN- and EC-Based Sensors

The size of the measuring spot of a sensor refers to the value of the radius or diameter of influence of the measurement device. The evaluated micromagnetic sensors (MBN and EC) have a gradient of the measured signal being maximal at the center. Determining the measuring spot size of sensors is crucial for two reasons: definition of the resolution for detection of gradations, and its effect on the sensor and closed-loop control dynamics. To determine the size of the measuring spot, a plate with 100% of martensite content was prepared and attached to a precision table equipped with a mechanism to perform axial displacements. The studied sensor heads were attached to a sensor holder and located over an area with no signal recording. Afterward, the sensors were turned on and moved horizontally in discrete steps of 0.5 mm toward the martensitic plate using the precision table (Figure 6a). The detected signals are measured during 60 s, producing plateaus in a plot of the recorded MBN or EC signals as a function of time. Then, the sensor is moved again 0.5 mm in horizontal direction and the new recorded signal is plotted as a new plateau during 60 s. This process must be repeated until a constant value of the measured signal is reached, which means that the maximum measurable signal or the center of the measuring spot is reached. Figure 6b illustrates an example of the obtained results for the 3MA-II sensor recording MBN signals. In

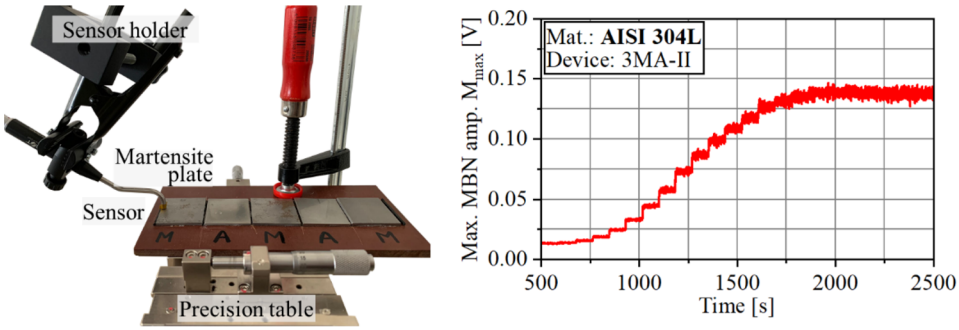


(a) (b)

**FIGURE 6** | Characterization of the radial size of the measuring spot: (a) experimental setup and (b) example of the obtained result for MBN measurements using the 3MA-II measuring system.

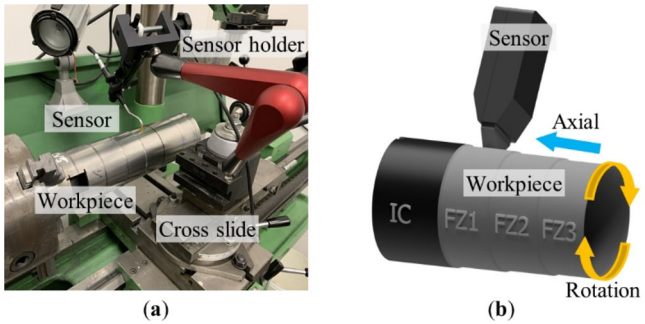


(a) (b)

**FIGURE 7** | Online detection of the amount of α′-martensite using MBN- and EC-based measuring systems: (a) experimental setup and (b) detail of the axial and rotational relative movements between sensor and workpiece.

this case, the last plateau is reached at around 1900 s and a total of 16 plateaus were measured. The number of plateaus multiplied by the 0.5 mm corresponds to the radial size of the measuring spot of the sensor.

### 2.4 | Experimental Setup for Online Measurements

Figure 7a illustrates the experimental setup to record online measurements using different measuring systems in a flow formed workpiece. A lathe machine was used to reproduce the relative movement between workpiece and sensor in a real flow forming process. Figure 7b shows in detail these movements: the rotation of the workpiece and the axial displacement that corresponds to the feed direction of the rolling tool during flow forming. To compare the performance of the sensors, the online measurements were performed during rotation of the workpiece, axial displacement of the sensor, and the combination of both of them.

The sensors were attached to a suitable sensor holder, which is connected to the cross slide of the lathe. For the rotational relative movement, the workpieces were set to rotate on the lathe at a speed of 90 rpm and the axial relative movements were generated by moving the cross slide at an approximated feed rate of 0.5 mm/s. Finally, measurements with a combination of rotation and axial displacement were recorded. The results were measured and reported for each forming zone separately.

## 3 | Results and Discussion

### 3.1 | Wall Thickness Reduction, Amount of α′-Martensite, and Average Roughness

Table 1 presents the quantitative results of measurements of wall thickness reduction ($\Delta w$), amount of α′-martensite, and average roughness (Ra) for the different forming conditions of the investigated workpiece. The ideal wall thickness reduction ($\Delta w_{ideal}$) refers to the infeed position of the roller tool to perform the forming operation. The real wall thickness reduction ($\Delta w_{real}$) is calculated from measurements on the produced specimen. The real values are slightly smaller than the ideal ones due to the behavior of the tool and the machine, as well as the material springback of AISI 304L [43]. The evolution of α′-martensite is consistent with the wall thickness reduction due to the amount of plastic deformation on each forming condition. At the IC, the measurement is around 0%—α′ and increases proportional to $\Delta w$, until a maximum of 91.5%—α′ is reached in FZ3.

The average roughness at IC has the minimum value since the nondeformed surface correspond to the raw material. Due to the movement of the roller tool during flow forming and the deformation, helical microgrooves appear. The feed rate of the tool defines the distance between the microgrooves (pitch of the helix) and the number of passes to perform the wall thickness reduction influences the depth of the microgrooves. Both aspects are determinant on the surface roughness of the components. Since the feed rate is kept constant, the roughness of the deformed surfaces is determined by the number of passes used during flow forming. As mentioned in Section 2.1, infeed depths of 0.75 mm/pass were applied. Therefore, FZ1 is formed in two passes of the roller tool, but FZ2 and FZ3 are formed in three and four passes, respectively. Therefore, the higher the number of passes the lower the depth of the microgrooves, which is reflected in lower roughness values. Therefore, the average roughness reaches the maximum at FZ1 with 2.8 µm and decreases until 2.3 µm at FZ3. These results are illustrated and summarized in Figure 8.

### 3.2 | Results of Measurements by Means of MBN-Based Sensors

The analysis of the results of this paper is focused on the evaluation of the sensitivity and dynamic conditions of the sensors to

**TABLE 1** | Quantitative results of measurements of wall thickness reduction, α′-martensite content, and average roughness of different forming conditions of the specimen used for the evaluation of the MBN- and EC-based measuring systems.

| Forming condition | Ideal wall thickness reduction $\Delta w_i$ [mm] | Real wall thickness reduction $\Delta w_r$ [mm] | α′-martensite content [%] | Average roughness Ra [µm] |
|---|---|---|---|---|
| IC | — | — | 0.175 | 1.243 |
| FZ1 | 1.50 | 1.01 | 35.13 | 2.843 |
| FZ2 | 2.25 | 1.59 | 73.08 | 2.512 |
| FZ3 | 3 | 2.19 | 91.53 | 2.353 |

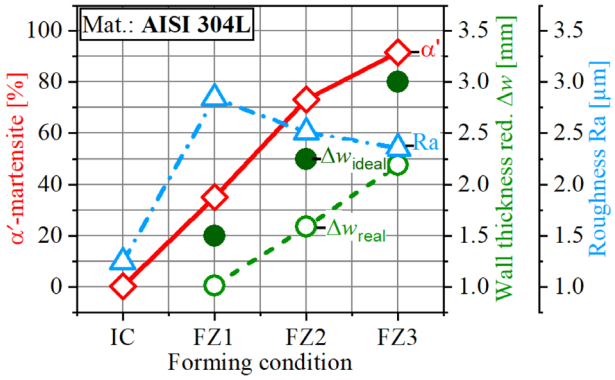


**FIGURE 8** | Results of amount of α′-martensite, wall thickness reduction, and average roughness for different forming conditions of the specimen used for the evaluation of the MBN- and EC-based measuring systems.

detect changes of magnetic properties in workpieces. The measurements were recorded online with relative motion between the sensor and the workpieces, reproducing the real conditions of production. As mentioned in Section 2.4, the relative movements correspond to the rotation of the workpiece, the axial displacement of the sensor, and the combination of them. It is widely documented that measurement systems operating under MBN and EC principles are suitable for detecting the evolution of magnetic properties due to phase changes [5, 40, 44]. Therefore, the calibration models for the conversion of measurements made with these devices into variables of interest, such as the amount of strain-induced α′-martensite, are not discussed in this paper.

Figure 9 summarizes the results of the recorded signals by means of the MBN measuring systems. The signals of 3MA-II and Rollscan 350 are qualitatively similar. The measured MBN micromagnetic parameters over the time on rotating workpieces show periodic peaks. Those peaks are due to the fact that the deformation-induced α′-martensite content around the workpiece is not completely uniform but has small variations. The deviations of the circularity of the tubes used as raw material cause that the contact conditions during flow forming are not uniform, therefore the formed α′-martensite is not constant around the surface of the tubes. From the point of view of the sensors, it is positive that both are sensitive to these small differences of the amount of α′-martensite during rotation.

The results show that the recorded signals for FZ3 can be fully differentiated from the measurements for FZ1 and FZ2. In contrast, the signals of FZ1 and FZ2 do not differ significantly and almost overlap with each other in all the relative movement conditions due to the effect of the surface roughness. As was demonstrated in earlier papers, higher roughness values increase the detected MBN signals [35, 45]. Higher roughness triggers the increment of the measured MBN signals, producing the mentioned overlap between FZ1 and FZ2, as well as an attenuation of the measured FZ3 signals. Since roughness cannot be measured online during the measuring process, their effects in a calibration model for the calculation of α′-martensite in terms of MBN measurements must be considered by means of other variables like feed rate. As discussed in Section 3.1, this parameter has a remarkable influence on the roughness.

In the measurements with only axial displacements, the peaks are not present in the recorded signals, since the workpiece does not rotate. The waviness of the measured signals is due to the cyclic nature of the MBN testing and the small discontinuities of the surface ought to the microgrooves created during production, as discussed before. The recorded signals increase slightly due to a small variation of the formed α′-martensite along each individual forming zone. The measurements with the combination of rotation of the workpiece and displacement of the sensors reveal a superposition of the signals explained above.

### 3.3 | Results of Measurements by Means of EC-Based Sensors

Figure 10 shows the recorded signals by means of the EC measuring systems.

The signals of 3MA-II and Elotest PL600 reveal that the three forming conditions are well differentiated from each other, since no overlapping of the signal is present in the plots. The recorded EC signals correlate qualitatively in a more reliable way with the measurements of α′-martensite. For instance, the plotted results of FZ2 are closer to FZ3 than to FZ1. This agrees with the measurements of α′-martensite reported in Table 1. From FZ1 to FZ2, the α′-martensite increases around 38% and from FZ2 to FZ3 only 18.5%. The periodical peaks on measurements of rotating workpieces were also recorded with EC-based measuring systems, which is a positive aspect regarding the sensibility to small variations of the magnetic properties. When the sensors are moved axially along the specimen, nearly constant signals are recorded. The results with the combination of both relative movements correspond to a superposition of the individual signals.

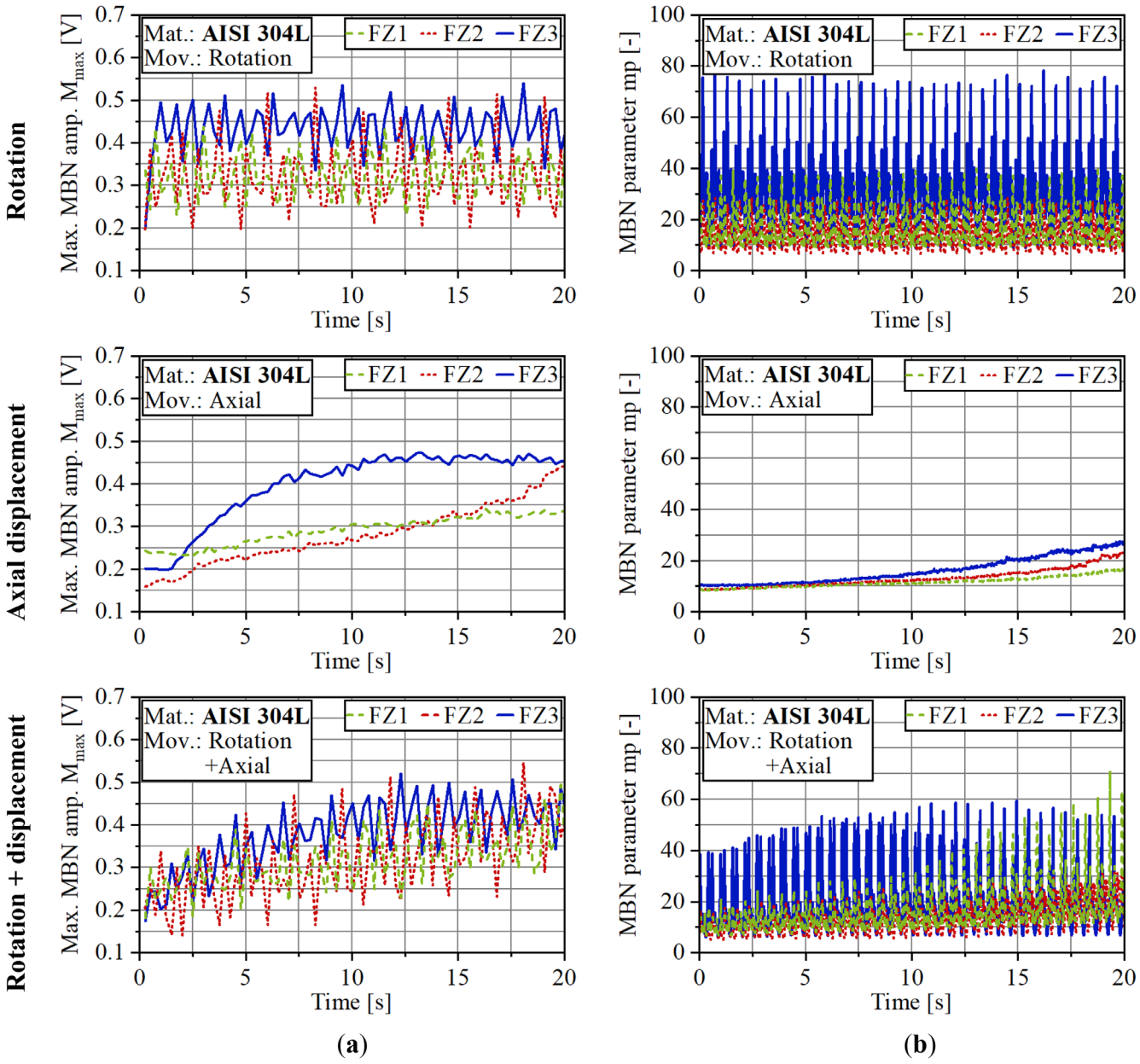


**FIGURE 9** | Results of online MBN measurements recorded during rotation of the workpiece, axial displacement of the sensor head, and the combination of both movements, using (a) 3MA-II and (b) Rollscan 350 measuring systems.

### 3.4 | Radial Size of the Measuring Spot of the MBN- and EC-Based Sensors

According to the procedure described in Section 2.3, the size of the measuring spot of the devices were calculated. Table 2 summarizes the results of the radial size of measuring spots for the investigated sensors. Although the 3MA-II system performs MBN and EC measurements, no difference of the radial size of the measuring spot was found between both methodologies.

A bigger radial size of the measuring spot implies a slower reaction of the sensor to changes of the conditions of the measured objects. Figure 11 shows a comparison of measurements recorded online in a transition zone between FZ2 and FZ3, using the 3MA-II and the Elotest PL600 sensors. The axial displacement of the sensor was carried out with the cross slide of the lathe at a speed of 0.5 mm/s. As expected, the Elotest PL600 sensor reacts quicker than 3MA-II to the changes of the amount of $\alpha'$-martensite. The reaction time is taken as the interval of time to reach two stable micromagnetic signals of the measured FZ2 and FZ3 conditions. The 3MA-II measuring systems take around 15 s to stabilize the signals, while Elotest PL600 takes around 7.5 s. Multiplying these values by the average horizontal speed used for measurements, yields values that are similar to those reported in Table 2 of the size of measuring spots of the sensors.

## 4 | Conclusions

The suitability of measuring systems operating on the principles of MBN and EC analyses for detection of the evolution of magnetic properties was investigated. The monitoring of

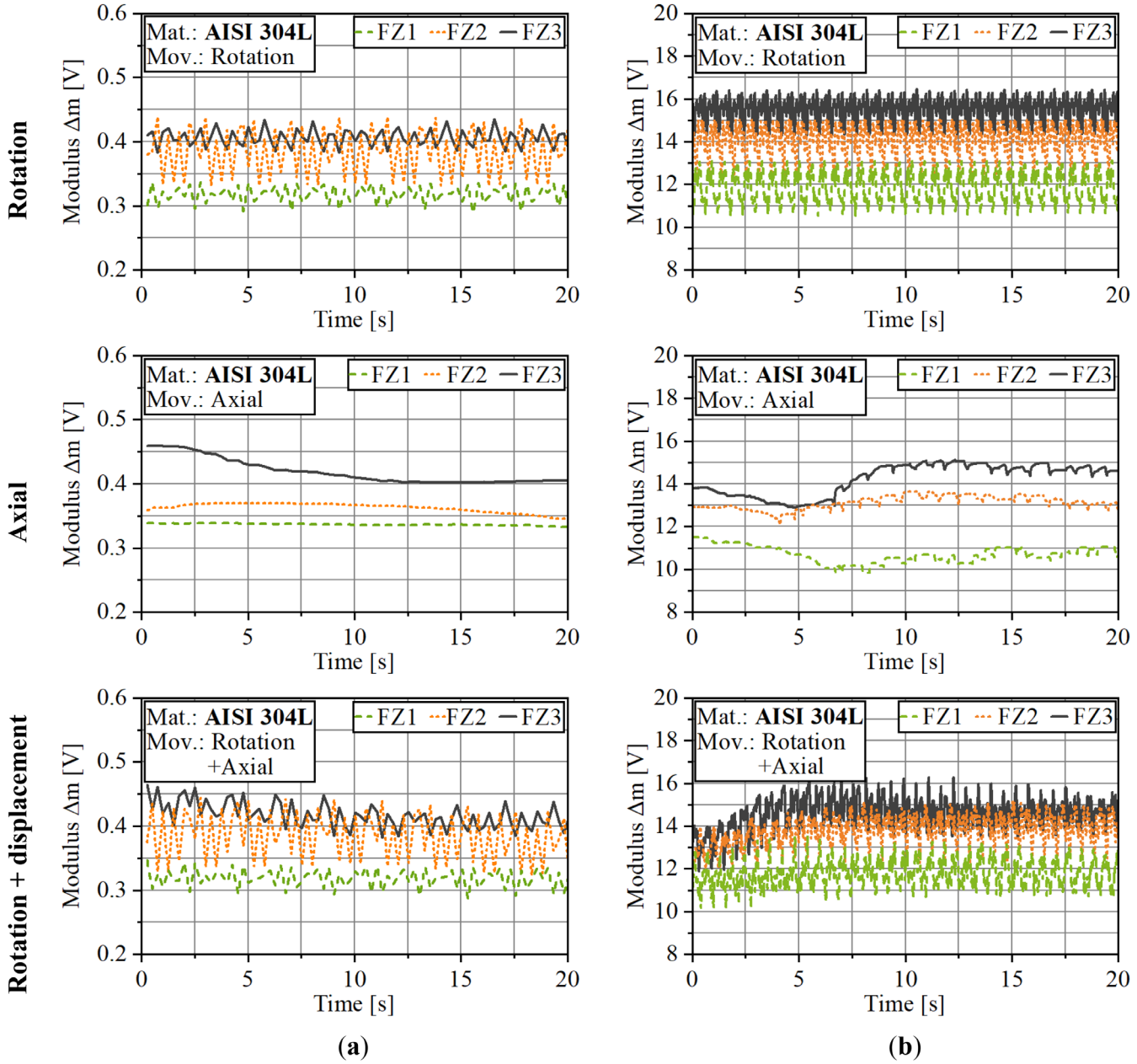


**FIGURE 10** | Results of online EC measurements recorded during rotation of the workpiece, axial displacement of the sensor head, and the combination of both movements, using (a) 3MA-II and (b) Elotest PL600 measuring systems.

**TABLE 2** | Radial size of the measuring spot of (a) 3MA-II, (b) Rollscan 350, and (c) Elotest PL600 measuring systems.

| (a) 3MA-II | (b) Rollscan 350 | (c) Elotest PL600 |
|---|---|---|
| 7.5 mm | 7.0 mm | 3.0 mm |

magnetic properties allows the detection of strain-induced α′-martensite during a property-controlled flow forming process. The assessment of the measuring systems was carried out emulating the real conditions during flow forming, regarding the relative motion between the workpiece and the sensor heads. Of each evaluated operating principle, the following devices were applied: 3MA-II that is capable to perform MBN and EC measurements at the same time, Rollscan 350 that carries out only MBN measurements and Elotest PL600 that is an EC-dedicated testing system. The results reveal that the main qualitative differences are between the measurement principles. Different devices working under the same operating principle deliver similar qualitative results. Both methodologies are suitable for online detection of α′-martensite amount through assessment of magnetic properties. However, the MBN-based sensors are more affected by the roughness of the measured surfaces. This does not mean that this type of sensor should be discarded to detect the amount of α′-martensite. As stated in the discussion of the results, sensor calibration models based on MBN analysis must consider the effects of roughness. The authors have already successfully applied such MBN sensors for α′-martensite detection using calibration models that take account of roughness by means of flow forming parameters such as feed rate [30].

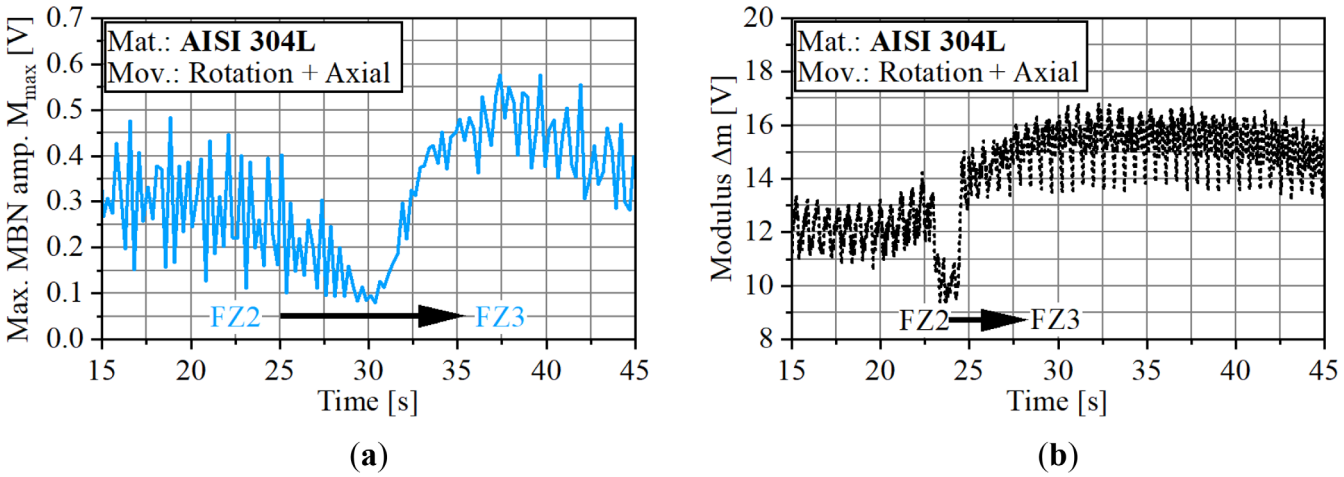


**FIGURE 11** | Results of online measurements in transition from FZ2 to FZ3 under combination of rotational and axial relative movement between sensor and workpiece, using (a) 3MA-II and (b) Elotest PL600 measuring systems.

The EC-based measurements are tightly correlated with the α′-martensite amount and are unaffected by other effects such as roughness. This entails that the calibration models to compute α′-martensite content do not require the inclusion of additional parameters to compensate for side effects. The investigation regarding the radial size of the measuring spot, reveals that the small size of the EC-dedicated device, represents an advantage with respect to the speed of reaction to the changes of the measured properties. This aspect is of great relevance for the characterization of the dynamic behavior of the sensors during the measurement process and the definition of their limitations for the detection of specially graded flow formed components.

The characterization of the measuring methodologies and sensors constitutes a milestone for the application of these systems under real production conditions in a property-controlled flow forming process. The study of their sensitivity to specific material properties and features allows to define operating windows, advantages, and limitations, which is fundamental in the development of calibration models and the use in the final applications.

### Author Contributions

**Julian Rozo Vasquez:** conceptualization, investigation, methodology, writing – original draft. **Hanigah Kanagarajah:** conceptualization, investigation, methodology, writing – original draft. **Bahman Arian:** software, writing – review and editing. **Lukas Kersting:** software, writing – review and editing. **Werner Homberg:** funding acquisition, project administration, validation, resources, supervision. **Ansgar Trächtler:** funding acquisition, project administration, validation, resources, supervision. **Frank Walther:** funding acquisition, project administration, validation, resources, supervision.


### Acknowledgments

The authors thank the German Research Foundation (Deutsche Forschungsgemeinschaft, DFG) for their support of the depicted research within the priority program SPP 2183 "Property-Controlled Forming Processes," through project no. 424335026 "Property Control During Spinning of Metastable Austenites." The authors thank too the Germany's Federal Ministry for Economic Affairs and Climate Action (BMWK) for funding the project "Development of a corrosion fatigue test rig to investigate the influences of copper-based alloys for hard metal/steel joints and the development of an adapted non-destructive testing methodology" (project no. KK5072219SH1) within the Central Innovation Program for small and medium-sized enterprises (ZIM) managed by AiF Projekt GmbH. Open Access funding enabled and organized by Projekt DEAL.


### Conflicts of Interest

The authors declare no conflicts of interest.

### Data Availability Statement

The data that support the findings of this study are available from the corresponding author upon reasonable request.

### References


1. D. Marini, D. Cunningham, P. Xirouchakis, and J. Corney, "Flow Forming: A Review of Research Methodologies, Prediction Models and Their Applications," *International Journal of Mechanical Engineering & Technology* 7, no. 5 (2016): 285–315.

2. M. Sohrabi, M. Naghizadeh, and H. Mirzadeh, "Deformation-Induced Martensite in Austenitic Stainless Steels: A Review," *Archives of Civil and Mechanical Engineering* 20, no. 4 (2020): 1–24, https://doi.org/10.1007/s43452-020-00130-1.

3. T. Angel, "Formation of Martensite in Austenitic Stainless Steels: Effects of Deformation, Temperature, and Composition," *Journal of the Iron and Steel Institute* 5 (1954): 165–174.

4. J. Allwood, S. Duncan, J. Cao, et al., "Closed-Loop Control of Product Properties in Metal Forming," *CIRP Annals* 65, no. 2 (2016): 573–596, https://doi.org/10.1016/j.cirp.2016.06.002.

5. N. Baak, R. Hajavifard, L. Lücker, et al., "Micromagnetic Approaches for Microstructure Analysis and Capability Assessment," *Materials Characterization* 178 (2021): 111189, https://doi.org/10.1016/j.matchar.2021.111189.

6. J. Rozo Vasquez, B. Arian, L. Kersting, W. Homberg, A. Trächtler, and F. Walther, "Qualification of Barkhausen Noise and Eddy Current Based Sensors for Online Monitoring of Strain-Induced α′-Martensite Formation During Flow Forming," in *Proceedings of Sensor and Measurement Science International SMSI2023 Conference* (Wunstorf, Germany: AMA Service GmbH, 2023), 197–198, https://goi.org/10.5162/SMSI2023/D1.1.

7. M. Roskosz, K. Fryczowski, and K. Schabowicz, "Evaluation of Ferromagnetic Steel Hardness Based on an Analysis of the Barkhausen Noise Number of Events," *Materials (Basel, Switzerland)* 13 (2020): 9, https://doi.org/10.3390/ma13092059.

8. S. Santa-aho, A. Sorsa, M. Honkanen, and M. Vippola, "Detailed Barkhausen Noise and Microscopy Characterization of Jominy End-Quench Test Sample of CF53 Steel," *Journal of Materials Science* 55, no. 11 (2020): 4896–4909, https://doi.org/10.1007/s10853-019-04284-z.

9. Z. Duan, Y. Kang, Y. Chen, Z. Wan, and S. Wang, "Reduction of Lift-Off Effect in Pulsed Eddy Current Testing for Surface Hardness Classification of Ferromagnetic Steel," *Measurement* 205 (2022): 112191, https://doi.org/10.1016/j.measurement.2022.112191.

10. S. Strodick, F. Vogel, M. Denstorf, et al., "Innovative X-Ray Diffraction and Micromagnetics Approaches for Reliable Residual Stress Assessment in Deep Rolled and Microfinished AISI 4140 Components," *Journal of Materials Research and Technology* 20 (2022): 2942–2959, https://doi.org/10.1016/j.jmrt.2022.07.168.

11. X. Liu, W. Shang, and C. He, "Effect of Microstructure and Residual Stress on the Magnetic Barkhausen Noise Signal," in *Proceedings of the 46th Annual Review of Progress in Quantitative Nondestructive Evaluation,14–19th July 2019, Portland, OR* (New York, NY: ASME Transactions, 2019).

12. P. Vourna, A. Ktena, P. Tsakiridis, and E. Hristoforou, "An Accurate Evaluation of the Residual Stress of Welded Electrical Steels With Magnetic Barkhausen Noise," *Measurement* 71 (2015): 31–45, https://doi.org/10.1016/j.measurement.2015.04.007.

13. J. Anglada-Rivera, L. Padovese, and J. Capó-Sánchez, "Magnetic Barkhausen Noise and Hysteresis Loop in Commercial Carbon Steel: Influence of Applied Tensile Stress and Grain Size," *Journal of Magnetism and Magnetic Materials* 231 (2001): 299–306.

14. A. Ktena, E. Hristoforou, G. Gerhardt, et al., "Barkhausen Noise as a Microstructure Characterization Tool," *Physica B* 435 (2014): 109–112, https://doi.org/10.1016/j.physb.2013.09.027.

15. J. Pal'a and J. Bydžovský, "Barkhausen Noise as a Function of Grain Size in Non-Oriented FeSi Steel," *Measurement* 46, no. 2 (2013): 866–870, https://doi.org/10.1016/j.measurement.2012.10.014.

16. E. Gorkunov, S. Zadvorkin, Mitropolskaya, D. I. Vichuzhanin, and K. Solov'ev, "Change in Magnetic Properties of Metastable Austenite Steel due to Elastoplastic Deformation," *Metal Science and Heat Treatment* 51, no. 9–10 (2009): 423–428.

17. M. Neslušan, J. Šugárová, P. Haušild, et al., "Barkhausen Noise Emission in AISI 321 Austenitic Steel Originating From the Strain-Induced Martensite Transformation," *Metals* 11, no. 3 (2021): 429, https://doi.org/10.3390/met11030429.

18. M. Teschke, J. Rozo Vasquez, L. Lücker, and F. Walther, "Characterization of Damage Evolution on Hot Flat Rolled Mild Steel Sheets by Means of Micromagnetic Parameters and Fatigue Strength Determination," *Materials* 13 (2020): 11, https://doi.org/10.3390/ma13112486.

19. L. Samfaß, N. Baak, R. Meya, O. Hering, A. Tekkaya, and F. Walther, "Micro-Magnetic Damage Characterization of Bent and Cold Forged Parts," *Production Engineering* 14, no. 1 (2020): 77–85, https://doi.org/10.1007/s11740-019-00934-y.

20. J. Dubec and M. Neslusan, "Multiparametric Analysis of Surface Integrity After Turning Through Barkhausen Noise in Relation to Tool Wear," *MM Science Journal* 2012 (July 2012): 314–317.

21. N. Baak, J. Nickel, D. Biermann, and F. Walther, "Barkhausen Noise-Based Fatigue Life Prediction of Deep Drilled AISI 4140," *Procedia Structural Integrity* 18 (2019): 274–279, https://doi.org/10.1016/j.prostr.2019.08.164.

22. N. Baak, J. Nickel, P. Starke, D. Biermann, and F. Walther, "Qualification of an Inner Surface Barkhausen Noise Sensor for Residual Stress Measurements of Single-Lip Deep Drilled AISI 4140 by Means of X-Ray Diffraction," in *Proceedings of the 13th International Conference on Barkhausen Noise and Micromagnetic Testing*, 23–24th September 2019, Prague, Czech Republic.

23. N. Baak, F. Schaldach, J. Nickel, D. Biermann, and F. Walther, "Barkhausen Noise Assessment of the Surface Conditions due to Deep Hole Drilling and Their Influence on the Fatigue Behaviour of AISI 4140," *Metals* 8, no. 9 (2018): 720, https://doi.org/10.3390/met8090720.

24. G. Dobman, I. Altpeter, B. Wolter, and R. Kern, "Industrial Applications of 3MA–Micromagnetic Multiparameter Microstructure and Stress Analysis," in *NDT.Net (Hrsg.)—Special Issue of e-Journal of Nondestructive Testing (eJNDT)* (Mayen, Germany: NDT.net, 2008).

25. I. Altpeter, "Industrial Integration of Residual Stress Measuring NDT-Systems Based on Ultrasonics and Micro-Magnetics," in *(Hrsg.)—AIP Conference Proceedings* (College Park, MD: AIP Publishing, 2005), 1387–1393, https://doi.org/10.1063/1.1916833.

26. G. Dobmann and B. Wolter, "Micromagnetic Testing for Rolled Steel," in *Proceedings of the 9th European Conference on NDT-ECNDT2006*, 25–29th September 2006, Berlin, Germany (Mayen, Germany: NDT.net, 2006), 1–11.

27. M. Deveci, "Detection Methods of Grinding Damages," Stresstech accessed October 3, 2023, www.stresstech.com/stresstech-bulletin-3-detection-methods-of-grinding-damages.

28. B. Karpuschewski, O. Bleicher, and M. Beutner, "Surface Integrity Inspection on Gears Using Barkhausen Noise Analysis," *Procedia Engineering* 19 (2011): 162–171, https://doi.org/10.1016/j.proeng.2011.11.096.

29. M. Riepold, B. Arian, J. Rozo Vasquez, W. Homberg, F. Walther, and A. Trächtler, "Model Approaches for Closed-Loop Property Control for Flow Forming," *Advances in Industrial and Manufacturing Engineering* 3 (2021): 100057, https://doi.org/10.1016/j.aime.2021.100057.

30. J. Rozo Vasquez, L. Kersting, B. Arian, W. Homberg, A. Trächtler, and F. Walther, "Soft Sensor Model of Phase Transformation During Flow Forming of Metastable Austenitic Steel AISI 304L," in *Numerical Methods in Industrial Forming Processes*, eds. J. Kusiak, Ł. Rauch, and K. Regulski (Cham: Springer International Publishing, 2024), 117–134, https://doi.org/10.1007/978-3-031-58006-2.

31. M. Astudillo, M. Nicolás, J. Ruzzante, et al., "Correlation Between Martensitic Phase Transformation and Magnetic Barkhausen Noise of AISI 304 Steel," *Procedia Materials Science* 9 (2015): 435–443, https://doi.org/10.1016/j.mspro.2015.05.014.

32. P. Haušild, K. Kolařík, and M. Karlík, "Characterization of Strain-Induced Martensitic Transformation in A301 Stainless Steel by Barkhausen Noise Measurement," *Materials & Design* 44 (2013): 548–554, https://doi.org/10.1016/j.matdes.2012.08.058.

33. J. Rozo Vasquez, H. Kanagarajah, B. Arian, et al., "Coupled Microscopic and Micromagnetic Depth-Specific Analysis of Plastic Deformation and Phase Transformation of Metastable Austenitic Steel AISI 304L by Flow Forming," *Practical Metallography* 59, no. 11 (2022): 660–675, https://doi.org/10.1515/pm-2022-0064.

34. J. Talonen, P. Aspegren, and H. Hänninen, "Comparison of Different Methods for Measuring Strain Induced α-Martensite Content in Austenitic Steels," *Materials Science and Technology* 20, no. 12 (2004): 1506–1512, https://doi.org/10.1179/026708304X4367.

35. J. Rozo Vasquez, B. Arian, M. Riepold, W. Homberg, A. Trächtler, and F. Walther, "Magnetic Barkhausen Noise Analysis for Microstructural Effects Separation During Flow Forming of Metastable Austenite 304L," in *Proceedings of the 11th International Work-Shop NDT in Progress, NDT in Progress 2021* (Mayen, Germany: NDT.net, 2021), 1–9. https://www.ndt.net/search/docs.php3?id=26462.

36. D. Jiles, *Introduction to Magnetism and Magnetic Materials* (London: Chapman & Hall, 1991).

37. B. Cullity and C. Graham, *Introduction to Magnetic Materials* (Piscataway, NJ, Hoboken, NJ: IEEE Press; Wiley, 2009).

38. S. Chikazumi, *Physics of Magnetism* (New York, NY, USA: John Wiley & Sons, Inc, 1966).

39. M. Seidel, W. Saxler, and B. Karpuschewski, *Schleifbrand und dessen Prüfung* (München: Hanser, 2020).

40. H. Stroppe and K. Schiebold, *Wirbelstrom-Materialprüfung* (Wuppertal: Castell-Verlag GmbH, 2011).

41. L. Fricke, H. Nguyen, J. Appel, et al., "Characterization of Deformation-Induced Martensite by Cryogenic Turning Using Eddy Current Testing," *Procedia CIRP* 108 (2022): 49–54, https://doi.org/10.1016/j.procir.2022.03.014.

42. B. Wolter, Y. Gabi, and C. Conrad, "Nondestructive Testing With 3MA—An Overview of Principles and Applications," *Applied Sciences* 9, no. 6 (2019): 1068, https://doi.org/10.3390/app9061068.

43. B. Arian, W. Homberg, J. Rozo Vasquez, F. Walther, M. Riepold, and A. Trächtler, "Forming of Metastable Austenitic Stainless Steel Tubes With Axially Graded Martensite Content by Flow-Forming," in *Proceedings of the 24th International Conference on Material Forming ESAFORM 2021,* 14–16th April 2021, Liège, Belgique (Liège, Belgium: University of Liège Library, 2021), https://doi.org/10.25518/esaform21.2759.

44. I. Altpeter, R. Tschuncky, and K. Szielasko, "Electromagnetic Techniques for Materials Characterization," in *Materials Characterization Using Nondestructive Evaluation Methods*, eds. G. Hübschen, H.-G. Herrmann, I. Altpeter, and R. Tschuncky (Cambridge, MA: Woodhead Publishing an imprint of Elsevier, 2016), 225–262.

45. M. Knyazeva, J. Rozo Vasquez, L. Gondecki, et al., "Micro-Magnetic and Microstructural Characterization of Wear Progress on Case-Hardened 16MnCr5 Gear Wheels," *Materials* 11 (2018): 11, https://doi.org/10.3390/ma11112290.